Astronomy in Focus, XXIXB, Focus Meeting 14
XXIXth IAU General Assembly, August 2015
Piero Benvenuti, ed.

doi:10.1017/S1743921316005482

Constraining Supermassive Black Hole Binary Dynamics Using Pulsar Timing Data

J. A. Ellis[1]† for the NANOGrav Collaboration

[1]Jet Propulsion Laboratory, California Institute of Technology, 4800 Oak Grove Drive, Pasadena, CA 91109, USA
email: Justin.A.Ellis@jpl.nasa.gov

Abstract. The most likely sources of nanohertz gravitational waves (GWs) are supermassive black holes (SMBHs) at the center of merging galaxies. A stochastic superposition of GWs from these sources is expected to produce a stochastic GW background that will leave a unique signature in the correlations of arrival times of pulses from a collection of radio pulsars. Using the 9-year data release from the North American Nanohertz Observatory for Gravitational Waves (NANOGrav) collaboration, we perform the first analysis that places constraints on the amplitude and *shape* of the stochastic GW background. We find that the data favor a turn over in the GW strain spectrum for current models of SMBH merger rates. This result indicates that environmental factors, other than GWs from circular binaries, are influencing the GW spectrum. Furthermore, we map constraints on the spectral shape to constraints on various environmental factors that drive the binary to the GW-driven regime including the stellar mass density for stellar-scattering, mass accretion rate for circumbinary disk interaction, and orbital eccentricity for eccentric binaries.

Keywords. Pulsars, Gravitational Waves

1. Introduction

This contribution is a summary of the extensive work presented in the recent NANOGrav 9-year Stochastic GW Background analysis (Arzoumanian *et al.* 2015).

Sazhin (1978) and Detweiler (1979) first realized that GWs could manifest as otherwise unexplained residuals in the times of arrival (TOAs) of pulsar signals after subtracting a deterministic *timing model*. Foster & Backer (1990) pointed out that the timing residuals from an array of pulsars (a *pulsar timing array*, or PTA) could be analyzed coherently to separate GW-induced residuals, which have distinctive correlations among different pulsars (Hellings & Downs 1983), from other systematic effects, such as clock errors or delays due to light propagation through the interstellar medium.

PTAs are most sensitive to GWs with frequencies on the order of the inverse timespan of timing observations, where TOA measurement noise averages out most efficiently. The strongest expected sources in this band are supermassive black hole binaries (SMBHBs) with masses of 10^8–$10^{10}\,M_\odot$, out to $z \simeq 1$ (Rajagopal & Romani 1995; Jaffe & Backer 2003; Wyithe & Loeb 2003). The binaries form after the hierarchical mergers (Sesana *et al.* 2004, 2008) of galaxies hosting individual SMBHs (as most galaxies are thought to do, cf. Kormendy & Ho 2013). Moreover, the cosmic population of SMBHBs may be observed collectively as a stochastic GWB composed of the incoherent superposition of signals from the binaries.

The simplest characterization of the stochastic GWB—a power-law Gaussian process with isotropic inter-pulsar correlations—applies if

† Einstein Fellow

(*a*) all binaries are assumed to have circular orbits (so each component signal is instantaneously monochromatic);

(*b*) all binaries evolve through the PTA band due purely to GW emission, as opposed to environmental effects such as interactions with nearby gas or with stars in the galactic nucleus;

(*c*) all binaries are distributed isotropically across the sky in sufficient numbers to fulfill the central limit theorem at all frequencies.

Under these conditions, the observed timing residuals due to the GWB are described fully by the (cross-) power spectral density

$$S_{ab}(f) = \Gamma_{ab} \frac{A_{\rm gw}^2}{12\pi^2} \left(\frac{f}{\rm yr^{-1}} \right)^{-\gamma} {\rm yr}^3, \tag{1.1}$$

where $A_{\rm gw}$ is the dimensionless strain amplitude, a and b range over the pulsars in the array, $\gamma = 13/3$ for a background composed of SMBHBs, and Γ_{ab} is the Hellings-Downs (1983) isotropic correlation coefficient for pulsars a and b. Power-law GWBs are also described (independently of observations) in terms of their *characteristic strain*

$$h_c(f) = A_{\rm gw} \left(\frac{f}{\rm yr^{-1}} \right)^{\alpha}, \tag{1.2}$$

which is related to Eq. 1.1 by $S_{ab}(f) = \Gamma_{ab} h_c(f)^2/(12\pi^2 f^3)$ and $\gamma = 3 - 2\alpha$ ($\alpha = -2/3$ for SMBHBs).

Recent predictions for the value of $A_{\rm gw}$, based on models of SMBH-galaxy coevolution and on observational constraints of galaxy assembly and SMBH mass functions, range between $\sim 10^{-15}$ and 10^{-14} (McWilliams *et al.* 2014; Sesana 2013a; Ravi *et al.* 2014)—hereafter MOP14, S13, and RWS14. Some of these models predict spectral densities that deviate from straight power-law behavior at low frequencies due to environmental couplings such as stellar scattering (Quinlan 1996) or circumbinary disk interaction (Ivanov *et al.* 1999); in that case, we refer the fiducial $A_{\rm gw}$ to their value at a frequency of 1 $\rm yr^{-1}$. Finally, recent observations, (Kormendy & Ho 2013), find higher black hole masses for a given host than previous work, indicating that an even stronger GWB may be expected; however, for this work we use the published results based on McConnell & Ma (2013) to make the most fair comparison among models.

2. Constraints on purely GW-driven background

Figure 1 shows the results of the power law and spectral analysis along with relevant astrophysical model predictions. The solid black and long dashed black lines are the 95% upper limits from the spectral and power-law analyses, respectively. The blue, gray, and red shaded regions are the one-sigma prediction on the strain spectra from MOP14, RWS14, and S13, respectively. We find an upper limit on the dimensionless strain amplitude of $A_{\rm gw} < 1.5 \times 10^{-15}$, slightly less constraining than the most stringent published upper limit to date (Shannon *et al.* 2015), and a factor of 2 more constraining than the recent EPTA upper limit (Lentati *et al.* 2015).

From inspection of Figure 1, our 95% upper limit is within the 1-sigma confidence regions of the S13 and RWS14 models and essentially rules out the MOP14 model under the assumption of a pure-powerlaw spectrum. This means that we are sensitive to a potential turnover in the spectrum due to environmental coupling factors. We wish to determine the level of consistency between our data and the power-law models displayed in Figure 1. To model the expected $A_{\rm gw}$ distributions, we use log-normal distributions

https://doi.org/10.1017/S1743921316005482 Published online by Cambridge University Press

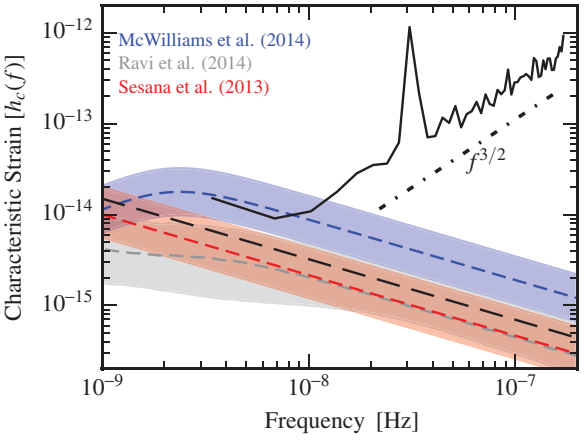

Figure 1. Strain amplitude vs. GW frequency. The solid black and long dashed black lines are the 95% upper limits from our spectral and power-law analyses. The red, gray and blue shaded regions are the one-sigma predictions from the models of S13, RWS14, and MOP14. The blue shaded region uses the simulation results from MOP14, but replaces the fit to the GWB predictions used in that paper with the functional form given by Eq. 3.3. The dash-dotted line shows the expected slope of the strain spectrum for white noise.

for the MOP14, S13, and RWS14, models. Since the models of RWS14 and S13 predict nearly the same GWB amplitude distribution (assuming a power-law only) we make no distinction between these two models. Furthermore, the model distributions on $A_{\rm gw}$, given by log-normal distributions have mean and standard deviations of $(-14.4, -15)$ and $(0.26, 0.22)$ for the MOP14 (hereafter Model A) and S13-RWS14 (hereafter Model B) models, respectively. Using the aforementioned distributions, we find that our data are 0.8% and 20% consistent with Models A and B, respectively, under the assumption of a power-law. This indicates that either the assumptions that go into these models are incorrect, our Universe contains a realization of the GWB that has an amplitude in the tail of the probability distributions mentioned above, or that environmental effects are depleting SMBHB sources at low frequencies making the power-law assumption faulty.

3. Constraints on a broken-powerlaw strain spectrum

One can place constraints on the shape of the GWB spectrum which could be due to environmental coupling effects that will likely affect our GWB signal at low frequencies (i.e., large orbital separations). We use a simple parameterization of the GWB spectrum that allows for a "bend" frequency at which there is a transition from environmentally-driven evolution to GW-driven evolution.

The characteristic amplitude of a stochastic background from an ensemble of SMBHBs in circular orbits is (Phinney 2001; Sesana *et al.* 2008; McWilliams *et al.* 2014)

$$h_c(f)^2 = \int_0^\infty dz \int_0^\infty d\mathcal{M} \frac{d^3N}{dz\, d\mathcal{M}\, dt} \frac{dt}{d\ln f} h^2(f), \tag{3.1}$$

where $d^3N/(dz\, d\mathcal{M}\, dt)$ is the differential number of inspiraling binaries per unit z, $\mathcal{M}$ and t, where z is the redshift, $\mathcal{M} = (m_1 m_2)^{3/5}/(m_1 + m_2)^{1/5}$ is the chirp mass of the binary, and t is the time measured in the binary rest frame. The $dt/d\ln f$ term describes the frequency evolution of the binary system, and $h(f)$ is the strain spectrum emitted by a single circular binary with orbital frequency $f/2$. Eq. 3.1 essentially contains two separable components that encode different physics. The $d^3N/(dz\, d\mathcal{M}\, dt)$ term encodes the

https://doi.org/10.1017/S1743921316005482 Published online by Cambridge University Press

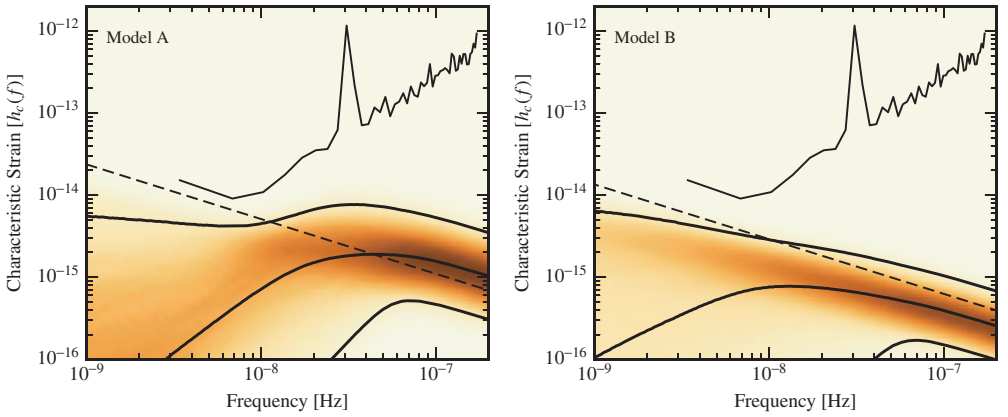

Figure 2. Probability density plots of the recovered GWB spectra for models A and B using the broken-power-law model parameterized by ($A_{\rm gw}$, $f_{\rm bend}$, and κ) as discussed in the text. The thick black lines indicate the 95% credible region and median of the GWB spectrum. The dashed line shows the 95% upper limit on the amplitude of purely GW-driven spectrum using the Gaussian priors on the amplitude from Models A and B, respectively. The thin black curve shows the 95% upper limit on the GWB spectrum from the spectral analysis.

galaxy coalescence rates and the black hole-host relations and the $dt/d\ln f$ encodes the physics of merging SMBHs including GW emission but also other physical mechanisms that are necessary to drive the binary coalescence and solve the so-called "final-parsec problem" (see Colpi 2014, for a review of SMBHB coalescence).

Following Sampson *et al.* (2015) we can generalize the frequency dependence of the strain spectrum to

$$\frac{dt}{d\ln f} = f\left(\frac{df}{dt}\right)^{-1} = f\left(\sum_i \left(\frac{df}{dt}\right)_i\right)^{-1}, \tag{3.2}$$

where i ranges over many physical processes that are driving the binary to coalescence. If we restrict this sum to GW-driven evolution and an unspecified physical process then the strain spectrum can be written

$$h_c(f) = A\frac{(f/f_{\rm yr})^{\alpha}}{\left(1+(f_{\rm bend}/f)^{\kappa}\right)^{1/2}}, \tag{3.3}$$

where $f_{\rm bend}$ and κ are the parameters that encode information about the physical processes (other than GW radiation) driving the binary evolution. Note here that the amplitude, A, is not strictly the same parameter as $A_{\rm gw}$ unless $f_{\rm bend} \gg 1/T$.

In the following analysis, we use the same log-normal distributions introduced in §2 for Models A and B as prior probability distributions for the GWB amplitude A in Eq. 3.3. In the following analysis we also fix $\alpha = -2/3$ but allow κ and $f_{\rm bend}$ to vary. Figure 2 shows the posterior probability density of the GWB spectrum defined in Equation 3.3 with Model A on the left and Model B on the right. The solid black lines in Figure 2 represent the 95% credible region and the median of the GWB spectrum. The dashed line is the upper limit on $A_{\rm gw}$ using the purely GW-driven spectrum (i.e., no transition frequency) and the Gaussian amplitude priors from Models A and B, respectively. Lastly the thin solid black line is the 95% upper limit on the GWB spectrum from the spectral analysis. Quantitatively, we find that the data prefer a turnover in the spectrum with Bayesian odds ratios of 22 and 2.2 to one for Models A and B, respectively.

https://doi.org/10.1017/S1743921316005482 Published online by Cambridge University Press

This analysis shows, for the first time, that PTAs are entering a regime where even in the case of a non-detection meaningful constraints can be placed on the dynamical history of the SMBHB population. Given a model for the SMBHB merger physics (i.e., a prior on A) and discarding the assumption of a purely GW-driven signal (i.e., a broken-power-law model), it is very difficult to rule out any of the GWB amplitude parameter space with any certainty unless one has strong *a priori* knowledge on the shape of the spectrum. However, we can begin to place constraints on the environmental coupling effects that drive the system to the GW-dominated regime.

4. Constraints on binary environmental influences

The cores of galactic merger remnants can harbor stars with little angular momentum and almost radial trajectories which intersect the central galactic region (centrophilic orbits). These stars can undergo three-body interactions with the resident SMBH binary, causing the stars to be ejected, which results in energy and angular momentum being extracted from the black hole system, and leading to binary hardening (Quinlan 1996).† Additionally, the formation of circumbinary gaseous disks can lead to interactions which extract energy and angular momentum from the binary orbit, driving it towards smaller orbital separations (Ivanov *et al.* 1999).

Both stellar scattering and circumbinary disk-interaction will cause a turnover in the GW strain spectrum that is dependent upon the physics driving the evolution. For stellar scattering the bend frequency can be written as

$$f_{\rm bend} \approx 3.25 \text{ nHz} \times \rho_3^{3/10} H_{15}^{3/10} M_8^{-23/50} q_r^{-3/10}, \tag{4.1}$$

where M is the total binary mass, $M_8 \equiv M/(10^8\ M_\odot)$, $q = M_2/M_1$, $q_r = q/(1+q)^2$, ρ is the mass density of stars, $\rho_3 \equiv \rho/(10^3\ M_\odot \text{pc}^{-3})$, H is the hardening rate, and $H_{15} \equiv H/15$. Here we have used the M-σ black hole-host relation of McConnell *et al.* (2011) but the dependence on this relation is weak. Furthermore, recent N-body scattering experiments (Sesana & Khan 2015) show that H is well constrained to $H \sim 15$. Astrophysical estimates on ρ are quite uncertain with estimated values around 10–$10^4\ M_\odot\ \text{pc}^{-3}$ for typical environments (Dotti *et al.* 2007). The variation of estimates over several orders of magnitude is why we choose to investigate only ρ in our stellar-scattering constraints.

The equivalent transition frequency for α-disk circumbinary interaction is

$$f_{\rm bend} \approx 0.144 \text{ nHz}\, M^{-17/14} q_r^{-6/7} \dot{M}_1^{3/7} a_0^{3/14}, \tag{4.2}$$

where a_0 is a characteristic orbital separation at which the enclosed disk mass equals the mass of the secondary black hole. In our constraints on the influence of circumbinary disk interactions, we only vary the accretion rate of gas onto the primary black-hole, $\dot{M}_1$, of which estimates in the literature vary over several orders of magnitude—typically $10^{-3} M_\odot\ \text{yr}^{-1}$–$1\ M_\odot\ \text{yr}^{-1}$ (e.g., Di Matteo *et al.* 2001; Armitage & Natarajan 2002; Goicovic *et al.* 2015).

The above relations for $f_{\rm bend}$ only apply to a single binary. By considering all binary environments to have the same ρ or $\dot{M}_1$, we can determine the spectral turnovers from the numerically computed strain spectra, iterating over many values of these environmental parameters to deduce a mapping.

† We assume that all galactic merger remnants maintain the same mass density of core stars throughout the binary merger. The subtleties of loss-cone replenishing impact the evolution of the binary and of the central density profile within a factor of ~ 2 (a few at most), as shown by Sesana & Khan (2015) and Vasiliev *et al.* (2015).

https://doi.org/10.1017/S1743921316005482 Published online by Cambridge University Press

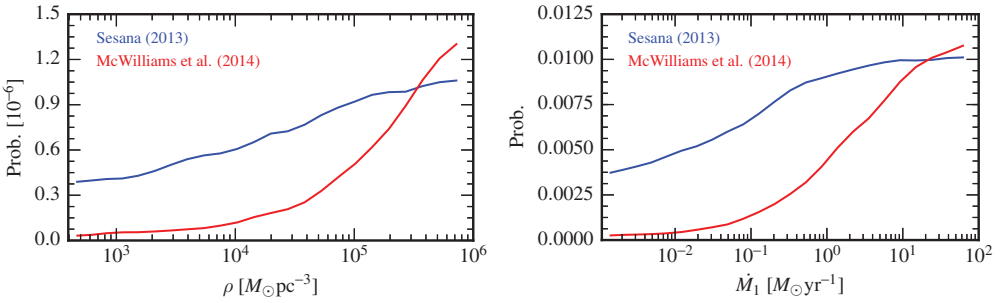

Figure 3. Posterior distributions for the mass density of stars in the galactic core (*left*) and the accretion rate of the primary black hole from a circumbinary disk (*right*).

In Fig. 3 we plot the posterior distributions of the stellar density, ρ, for stellar hardening, and mass accretion rate, $\dot{M}_1$ for circumbinary disk interaction. In this analysis we perform the Bayesian parameter estimation for fixed values of κ corresponding to the appropriate values for stellar hardening ($\kappa = 10/3$) and circumbinary disk interaction ($\kappa = 7/3$). These posteriors are constructed by using the empirical mapping discussed above to convert $f_{\rm bend}$ to the appropriate astrophysical parameter. From inspection of Fig. 3 we see that the MOP14 model heavily prefers $\rho \gtrsim 10^4\ M_\odot{\rm pc}^{-3}$ and $\dot{M}_1 \gtrsim 10^{-1}\ M_\odot{\rm yr}^{-1}$, while the S13 model is largely unconstraining for both mechanisms.

Typical densities of massive elliptical galaxies at the MBH influence radius is $\sim 10^3\ M_\odot\ {\rm pc}^{-3}$, making the MOP14 model hard to reconcile with observations, even if we consider that massive ellipticals were likely a factor of 2–3 more compact at $z = 1$ (Sesana, priv. comm.). Our results approach the upper end (for the MOP14 prior) of the expected range of $\dot{M}$, $10^{-3} M_\odot\ {\rm yr}^{-1}$–$1\ M_\odot\ {\rm yr}^{-1}$, observed in the local Universe and predicted via simulations, see e.g. Di Matteo *et al.* 2001; Armitage & Natarajan 2002; Goicovic *et al.* 2015. Furthermore, Dotti *et al.* (2015) predict that $\dot{M}_1 \ll 10^{-1}\ M_\odot\ {\rm yr}^{-1}$ for BH masses of $10^9\ M_\odot$ and redshifts $z < 1$; however, these are average accretion rates, and short, episodic accretion triggered by galaxy mergers could occur at a higher rate.

Above we have considered environmental effects for *circular* orbits, in reality, the history of a binary's eccentricity will see phases of growth and circularization depending upon the interplay of environmental factors and GW emission (e.g., Sesana 2010; Kocsis & Sesana 2011). Thus the binary could come into the PTA frequency band with non-negligible eccentricity. The cumulative effect over the entire population can lead to a depletion of the low frequency strain spectrum (Enoki & Nagashima 2007; Sesana 2013b; Ravi *et al.* 2014; Huerta *et al.* 2015) with a turnover. We construct eccentric populations and corresponding strain spectra using the formalism of Huerta *et al.* (2015). The inferred posteriors on the eccentricity of all binaries at a semi-major axis of 0.01 pc from this mapping is shown in Fig. 4. The MOP14 prior leads to an eccentricity posterior distribution that largely favors $e_0 \gtrsim 0.7$ while the S13 prior leads to an eccentricity posterior that is consistent with smaller eccentricities, more weakly favoring $e_0 \gtrsim 0.5$. We emphasize that, whilst these eccentricities seem rather large, it is well established that binaries evolving in stellar environments tend to increase their eccentricity (Quinlan 1996). It is therefore likely that most binaries can get to $e \sim 0.5$–0.7 along their evolution (see tracks in Sesana 2010). The eccentricity growth rate is generally larger for smaller binary mass ratios, and for larger initial eccentricities. The latter is indeed a crucial parameter; if, following galaxy mergers, the SMBHB already has a significant ($e \gtrsim 0.5$) eccentricity at the moment of formation, the subsequent evolution will almost certainly drive it to $e > 0.9$. Given that the SMBHB eccentricity at formation is hard to

https://doi.org/10.1017/S1743921316005482 Published online by Cambridge University Press

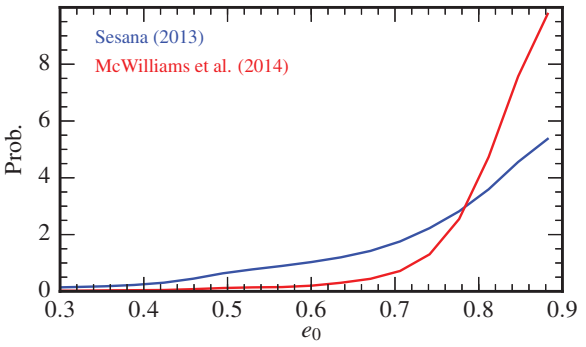

Figure 4. Same as Figure 3 except now we display posterior distribution for the eccentricity of SMBH binaries when they had a semi-major axis of 0.01 pc.

determine (Aarseth 2003; Hemsendorf *et al.* 2002; Berentzen *et al.* 2009; Amaro-Seoane *et al.* 2009), it is impossible to draw astrophysical conclusions from the constrains above. Nonetheless, this is strong evidence against the circular binary hypothesis.

5. Conclusions

The results presented here, and described in further detail in Arzoumanian *et al.* (2015), have shown

- For optimistic and standard models of galactic merger rates and black hole-host relations, our data favor a turnover in the spectrum of the nanohertz stochastic gravitaitonal-wave signal with odds ratios of 22:1 and 2:1, respectively.
- The existence of a spectral turnover in the nanohertz band shows that either (i) supermassive black-hole binaries are not all circular and radiation-reaction driven, or (ii) a significant fraction of all binaries stall at orbital separations too large to allow radiation-driven merging within a Hubble time.
- Scenario (i) implies that supermassive black-hole binaries may be strongly coupled to and driven by their local astrophysical environment, allowing us to perform the first gravitational-wave investigations into dynamical processes in galactic nuclei currently proposed to ameliorate the "final parsec problem" of galaxy formation.
- Assuming negligible stalling, the paradigm of circular, radiation-reaction driven supermassive black-hole binaries in the nanohertz GW band is thrown into considerable doubt by pulsar-timing arrays.

Acknowledgement

The NANOGrav project receives support from National Science Foundation (NSF) PIRE program award number 0968296 and NSF Physics Frontier Center award number 1430284. JAE acknowledges support by NASA through Einstein Fellowship grant PF4-150120.

References

Aarseth, S. J. 2003, *Ap&SS*, 285, 367
Amaro-Seoane, P., Miller, M. C., & Freitag, M. 2009, *ApJ*, 692, L50
Armitage, P. J. & Natarajan, P. 2002, *ApJ*, 567, L9
Arzoumanian, Z., *et al.* The NANOGrav Collaboration 2015, *ApJ*, in press; arXiv:1508.03024
Berentzen, I., Preto, M., Berczik, P., Merritt, D., & Spurzem, R. 2009, *ApJ*, 695, 455

Colpi, M. 2014, *Space Sci. Rev.*, 183, 189
Detweiler, S. 1979, *ApJ*, 234, 1100
Di Matteo, T., Carilli, C. L., & Fabian, A. C. 2001, *ApJ*, 547, 731
Dotti, M., Colpi, M., Haardt, F., & Mayer, L. 2007, *MNRAS*, 379, 956
Dotti, M., Merloni, A., & Montuori, C. 2015, *MNRAS*, 448, 3603
Enoki, M. & Nagashima, M. 2007, *Prog. Theor. Phys.*, 117, 241
Foster, R. S. & Backer, D. C. 1990, *ApJ*, 361, 300
Goicovic, F. G., Cuadra, J., Sesana, A., *et al.* 2015, *MNRAS*; submitted; arXiv:1507.05596
Hellings, R. W. & Downs, G. S. 1983, *ApJ*, 265, L39
Hemsendorf, M., Sigurdsson, S., & Spurzem, R. 2002, *ApJ*, 581, 1256
Huerta, E. A., McWilliams, S. T., Gair, J. R., & Taylor, S. R. 2015, *Phys. Rev. D*, 92, 063010
Ivanov, P. B., Papaloizou, J. C. B., & Polnarev, A. G. 1999, *MNRAS*, 307, 79
Jaffe, A. H. & Backer, D. C. 2003, *ApJ*, 583, 616
Kocsis, B. & Sesana, A. 2011, *MNRAS*, 411, 1467
Kormendy, J. & Ho, L. C. 2013, *ARA&A*, 51, 511
Lentati, L., *et al.* 2015, *MNRAS*, 453, 2576
McConnell, N. J. & Ma, C.-P. 2013, *ApJ*, 764, 184
McConnell, N. J., Ma, C.-P., Gebhardt, K., *et al.* 2011, *Nature*, 480, 215
McWilliams, S. T., Ostriker, J. P., & Pretorius, F. 2014, *ApJ*, 789, 156 (MOP14)
Phinney, E. S. 2001, astro-ph/0108028
Quinlan, G. D. 1996, *New Astron.*, 1, 35
Rajagopal, M. & Romani, R. W. 1995, *ApJ*, 446, 543
Ravi, V., Wyithe, J. S. B., Shannon, R. M., Hobbs, G., & Manchester, R. N. 2014, *MNRAS*, 442, 56 (RWS14)
Sampson, L., Cornish, N. J., & McWilliams, S. T. 2015, *Phys. Rev. D*, 91, 084055
Sazhin, M. V. 1978, *Soviet Ast.*, 22, 36
Sesana, A., Haardt, F., Madau, P., & Volonteri, M. 2004, *ApJ*, 611, 623
Sesana, A. 2010, *ApJ*, 719, 851
Sesana, A. 2013a, *MNRAS*, 433, L1 (S13)
Sesana, A. 2013b, *Classical Quant. Grav.*, 30, 224014
Sesana, A. & Khan, F. M. 2015, *MNRAS*, 454, L66
Sesana, A., Vecchio, A., & Colacino, C. N. 2008, *MNRAS*, 390, 192
Shannon, R. M., *et al.* 2015, *Science*, 349, 1522
Vasiliev, E., Antonini, F., & Merritt, D. 2015, *ApJ*, 810, 49
Wyithe, J. S. B. & Loeb, A. 2003, *ApJ*, 590, 691